Production of Radioactive Nuclides in a Lead Assembly with 500 MeV Protons

H. Takada, I. Kanno †, K. Hasegawa and T. Sasa

Japan Atomic Energy Research Institute
Tokai-mura, Naka-gun, Ibaraki-ken,
319-11, Japan

I. Introduction

It is a current interest to transmute long-lived radioactive wastes by the use of an intense proton accelerator. There proposed several concepts for the accelerator-based transmutation system.[1-3] Since these systems are driven by the proton induced spallation neutrons in a target, the neutron yield and the neutron spectrum from the thick target are important factors to decide the performances of the systems.

Because the evaluated nuclear data files are not prepared for the energy region above 20 MeV, nucleon meson transport codes([4]) were used to neutronics calculation in the design studies. In these codes the spallation reactions and the transport of the particles are simulated by the intranuclear cascade evaporation (INCE) model.[5] It was indicated by recent works[6,7] that the INCE model reproduced neutron emission from thin target well, although the model underestimated the backward component of the double differential cross sections.

From the viewpoints of the target design, it is necessary to know the validity of the codes in comparison with thick target experiments. Several integral experiments[8-13] were carried out to study the leakage neutron spectrum, the neutron yield and the nuclide production for the medium energy protons incidence.

In this work, an integral experiment was performed to understand the transport of the spallation neutrons using a lead assembly, which can be regarded as a mockup of the transmutation system[3] based on the fast neutrons. In the experiment, several kinds of activation samples were inserted into the assembly and were irradiated with 500 MeV protons. The number of induced nuclides was obtained by y-ray measurements.

---

† Present Address : Kyoto University, Yoshida-Honcho, Sakyo-ku, Kyoto, 606, Japan

Preliminary calculation was also performed using the nucleon meson transport code NMTC/JAERI[4]. The calculated results were compared with the experimental ones.

2.Experimental Procedure

In the experiment, the lead assembly was irradiated at the beam dump room of the 500 MeV booster proton synchrotrons facility of National Laboratory for High Energy Physics. Figure 1 shows the cross section of the lead assembly. The size of the assembly was 60 cm in diameter and 100 cm in length. The 500 MeV protons were injected into the assembly through the hole of 16 cm in diameter and 20 cm in length.

The activation samples were inserted into the lead assembly along the beam axis at the position of O, 3,6, 10, 15,20 and 25 cm. The purities of the samples were as follows: A1(99.999%), Fe(99.99%), Ni(99.9%), Cu(99,99%), Au(99.999%) and Pb(99.99%). The size of the sample was 6 mm in diameter and 10 mm in length, respectively.

The lead assembly was irradiated with 6.3x1014 to 3.3x10[1]5 protons. The number of the protons was monitored by the pickup coil, the activation foil of Al and the faraday cup. After 30 hours cooling, y-ray measurement was started with a Ge-detector (relative efficiency of 20% to 3“x3” NaI scintillation detector). The measured data were taken on the computer by 4k channels and were analyzed by the program BOB([14]). The reaction rate was obtained by the following relation:

$$Y_j exp = \frac{\lambda_j I_j}{\varepsilon_j \eta \delta P N (1-e^{-\lambda_j Tr}) e^{-\lambda_j Tc} (1-e^{-\lambda_j Tm})}, \qquad (1)$$

where j : jth produced nuclide,

λ_j : the decay constant,

I_j : the peak area,

P : the number of protons,

N: the number of atoms in an activation sample,

ε_j : the peak efficiency of the Ge-detector,

η : the number of photons emitted per decay,

δ : the self-absorption for photons in an activation sample,

Tr: the irradiation time,

Tc: the cooling time and

Tm: the measuring time.

The peak efficiency ε_j was determined by the calibrated gamma sources of ^{22}Na, ^{60}Co, ^{137}Cs and ^{152}Eu. The self absorption for photons in an activation sample δ was calculated by Monte Carlo method assuming that the photons were produced uniformly in the sample. The uncertainties for the decay constant and the number of photon per decay were not included in this estimation. Table 1 summarizes the errors with respect to the γ-ray measurement.

3. Nucleon Transport Calculation

Preliminary calculation was performed to compare the results with the experimental ones. The reaction rate $Y_j cal$ was evaluated by the following equation :

$$Y_j cal = \sum_i \int_{Eth}^{500} \sigma^i_j(E)\phi^i_j(E)dE \quad , \quad (2)$$

where i stands for proton or neutron, $\sigma^i_j(E)$ is the production cross section for the nuclides j, $\phi^i_j(E)$ the flux of nucleon i and Eth the threshold energy. In this calculation, the reaction rate was calculated by dividing the energy range into some groups:

$$Y_j cal = \sum_i \sum_g \sigma^i_{j,g}\ \phi^i_{j,g} \quad , \qquad (3)$$

where, g indicates the number of energy group. The group structure is shown in Table 2.

The nucleon flux was calculated by the code NMTC/JAERI for the homogeneous lead assembly on condition that the number of history was 100,000 and that the cut off energy for the nucleon transport was 15 MeV. The beam profile was assumed to be the gaussian configuration which was obtained by the yield of 24Na in the Al foil at the beam entrance hole. The profile of 24Na yield in the Al foil is shown in Figure 2.

As for the activation cross section, the experimental data(15-17) were employed for proton induced reaction. For neutron induced reaction, on the other hand, the calculated values were employed because of lack of the experimental neutron induced activation cross sections above 20 MeV. We evaluated the cross section using NMTC/JAERI.

4. Results and Discussions

In this experiment, we identified the nuclide whose half life is beyond 10 hours. Major identified nuclides are summarized in Table 2 for Al, Fe, Ni and Cu samples.

Figure 3 shows the spatial distribution of the reaction rate of ^{206}Bi produced in lead samples. Figure 4 exhibits the proton fluence calculated using NMTC/JAERI by the surface cross estimation method. Since the range of the 500 MeV proton is 20 cm in the lead, the calculated proton fluence decreases rapidly at 20 em in depth. It is clearly seen from Figure 4 that ^{206}Bi was produced even in the position beyond 20 cm on the axis. This fact indicates that the streaming of the high energy protons between the samples and the lead assembly might occur along the axis. As for the ^{206}Bi production at r=3 cm, the measured data exhibited similar behavior as the calculated results, although significant peak was seen around 20 cm in depth.

Figure 5 shows the spatial distribution of the reaction rate of 57Ni produced in the nickel samples. The measured data seemed to be the typical profile of the intensity of the induced nuclides in the lead assembly. Since the protons was incident on the surface at 20 cm in depth, the reaction rate shows the greatest value at the position and decrease exponentially. It should be noticed that the production of 57Ni, was observed at the position of r= 25 cm. Because the threshold energy of the 57Ni production is 12.4 MeV, it is indicated that the fast neutrons transported to the periphery of the lead assembly.

In Figure 6, the measured reaction rates for ^{57}Co, 56C0 and ^{55}Co produced in the copper samples are compared with the calculated ones. For these nuclides, the threshold energies have almost same values of 28, 35 and 30 MeV. On the other hand, the cross sections are 16.8, 5.2 and 1.2 mb for proton incidence, respectively.(18) Consequently, the measured data indicated the difference of the activation moss section among the nuclides implicitly. Comparing the results of the position of r=3 cm with those on the axis, it is possible to say that the ratio of the activation cross sections between the cobalt isotopeare larger for neutron incidence than for proton incidence.

The calculated results reproduced the measured data well at r=3 cm, although some discrepancy was seen for 57C0 production. On the axis, however, the calculated results can not evaluate the measured data at the position deeper than 20 cm at all. There may be at least two reasons for the discrepancy. One is that the NMTC/JAERI could not estimate the angular distribution of the nucleons in the simulation of nuclear reactions correctly. Another one is that the measured data might include the contribution of the streaming of “the high energy protons.

In Figure 7, the measured reaction rates for 5^4Mn and 52Mn produced in the copper samples are compared with the calculated ones. For these nuclides, the threshold energies

are 50 and 67 MeV and the cross sections are 7.2 and 2.7 MeV, respectively. In this case, the calculated results agreed with the measured data fairly well for ^{52}Mn production at r=3 cm. As for 5^{4}Mu production, however, the calculation underestimated the measured data by a few times in magnitude. The disagreements might be attributed to the underestimation of the activation cross section for neutron incidence.

In Figures 8 and 9, the measured reaction rates for 5^{2}Mn and ^{4}8V produced in the iron samples are compared with the calculated results. For the ^{4}8V production, the threshold energies is 35 MeV, which is the same value as the reaction ^{nat}Cu(n, x)^{56}Co. From Figure 6 and 9, the reaction '^{at}Fe(n, x)^{48}V seemed to have almost equal cross section as the reaction ^{nat}Cu(n, x)^{56}Co. The calculated results exhibited similar behavior for the iron samples as is seen in the results of the copper samples at r=3 cm. Good agreements were obtained between the calculated and the measured results at r=6 cm for both nuclides.

In Figures 10 through 12, the measured reaction rates for 56Ni, 52Mn and ^{4}8V produced in the nickel samples are compared with the calculated results. For these nuclides, the threshold energies are 23,40 and 60 MeV, respectively. In these Figures, one can see fairly good agreements at the position of r=3 to 10 cm between the calculated and the measured results for 56Ni and ^{4}8V production, respectively. For ^{52}Mn production, however, the calculation could not reproduce the measured data even in the position where the radial distance is greater than 3 cm. The fact might be caused to the poor estimation of the activation cross section for the reaction 'atNi(n,x)^{52}Mn.

Since the calculated activation cross sections were used to estimate the reaction cross section in this work, it is necessary to know the validity of the codes. In Figures 13 and 14, the calculated excitation functions are compared with the experimental ones(15-17) for proton incident reactions. There exists the discrepancies of a couple of times in magnitude. between the calculated and the experimental ones. It is considered from these results that the degree of the agreement seen in the Figures 6 though 12 will be in the reasonable range. It is necessary to investigate the activation cross sections to make more sophisticated discussions.

5. Summary

An integral experiment was performed to study the transport of the spallation neutrons in the lead assembly using 500 MeV protons. Spatial distributions of the reaction rates of the induced radioactive nuclides were obtained using various activation samples. Measured data were compared with the results of the nucleon-meson transport code

NMTC/JAERI. The calculated results agreed with the measured ones fairly well at the position of 3,6 and 10 cm in radial distance. However, NMTC/JAERI underestimated the results on the axis beyond 20 cm in depth. In order to compare the results in detail, further investigations will be required from experimental and calculational aspects with respect to the production cross section and to the streaming effect on the axis.

Acknowledgement

This work was carried out under the contract for the use of the booster synchrotrons facility of National Laboratory for High Energy Physics. The authors wish to gratefully acknowledge Prof. N. Watanabe and the staffs of National Laboratory for High Energy Physics for their support to the experiment. We also thank Drs. M. Mizumoto and H. Yasuda for their useful discussions and encouragement for the experiment. We are also indebted to Drs. Y. Nakahara and T. Nishida for their helpful comments with regard to the calculation. Mr. T. Ono and Mr. M. Takeuchi are also thankful for their help for the experiment.

References

(1) E. D. Arthur: Proc. of 6th Int. Conf. Emerging Nucl. Energy Systems, Fusion Technol., 20, Part 2, 641(1991)
(2) H. Takahashi: ibid., p657
(3) H. Takada, et al.: ibid., p673
(4) For example, Y. Nakahara and T. Tsutsui: JAERI-M 82-198 (1982), (in Japanese).
(5) H. W. Bertini: Phys. Rev. 131, 1801(1963).
(6) M. M. Meier, et al.: Nucl. Sci. Eng. 102, 310(1989).
(7) M. M. Meier, et al.: Nucl. Sci. Eng. 110, 289(1989).
(8) Y. Arakita, et al.: Nucl. Instr and Meth. 164,225 (1979)
(9) R. G. Vasil'kov, et al.: Atomnaya Energiya 44,329 (1978)
(10) S. S. Cierjacks, et al.: Jul-Conf-45, 215 (1981)
(11) F. Raupp, et al.: Jul Conf-45, 333 (1981)
(12) G. G. Russel: Jul-Conf-45, 621 (1981)
(13) R. G. Vasil'kov and V. I. Yurevich: Proc. of 1 1th Int. Collaboration on Advanced Neutron Sources, KEK-Report 90-25, 340(1990)
(14) H. Baba: JAERI-M 7017 (1977).
(15) R. Michel., H. Weigel and W. Herr: Z. Phys. A286, 393 (1973).
(16) R. Michel, et al.: Nucl. Phys.A322 40 (1979).

(17) R. Michel and R. Stuck.: J. Geophys. Res. 89, B673 (1984).
(18) J. T. Routti, Physics Scripts, 10, 107(1974)

Table 1. Estimated experimental errors.

Items	Estimated errors (?6)
1. Number of protons	10
2. Statistics of peak area	<1 to 34.4
3. Peak efficiency	2.0 to 4.0
4. Number of atoms in the sample	<0.5
5. Times for irradiation, cooling and measuring	< 0.5

Table 2. Group structure for reaction rate calculation.

Group No.	Lower Energy (MeV)	Group No.	Lower Energy (MeV)
1	15	12	90
2	20	13	100
3	25	14	120
4	30	15	140
5	35	16	160
6	40	17	180
7	45	18	200
8	50	19	250
9	60	20	300
10	70	21	400
11	80		

Table 3. Identified nuclides in the samples of Al, Fe, Ni and Cu.

Samples	Identified Nuclides
Al	7Be, ^{2}2Na, 2^{4}Na
Fe	42K, 43K, ^{44m}Sc, ^{46}Sc, ^{48}V, ^{48}Cr, ^{51}Cr, 52Mn, 54Mn,56Co
Ni	42K, 43K, ^{44m}Sc, ^{46}Sc, ^{48}V, ^{48}Cr, ^{51}Cr, ^{52}Mn, ^{54}Mn, 52Fe, ^{59}Fe, ^{55}Co, 56Co, 57 Co, ^{58}Co, 56Ni, 57Ni
Cu	42K, 43K, ^{44m}Sc, ^{46}Sc, ^{48}V, ^{48}Cr, ^{51}Cr, ^{52}Mn, ^{54}Mn, ^{59}Fe, ^{55}Co, ^{56}Co, ^{57}Co, ^{58}Co, 56Ni, 57Ni, ^{62}Zn, ^{65}Zn

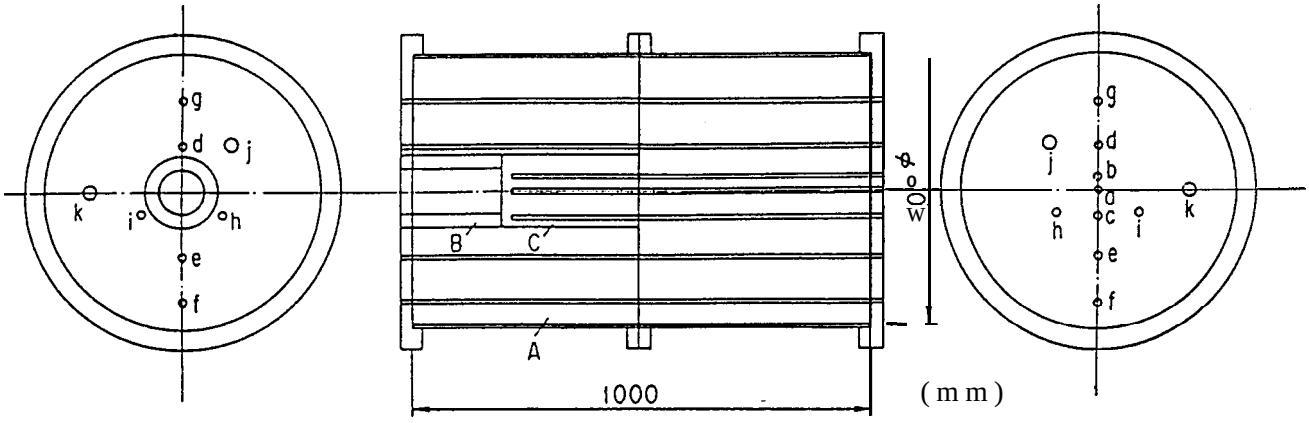

Figure 1. Cross sectional view of the lead assembly. The small holes (a to i) indicate the places where activation samples are inserted. The capitals A stands for the lead assembly, B the beam entrance hole, C the lead target which can be replaced with different one.

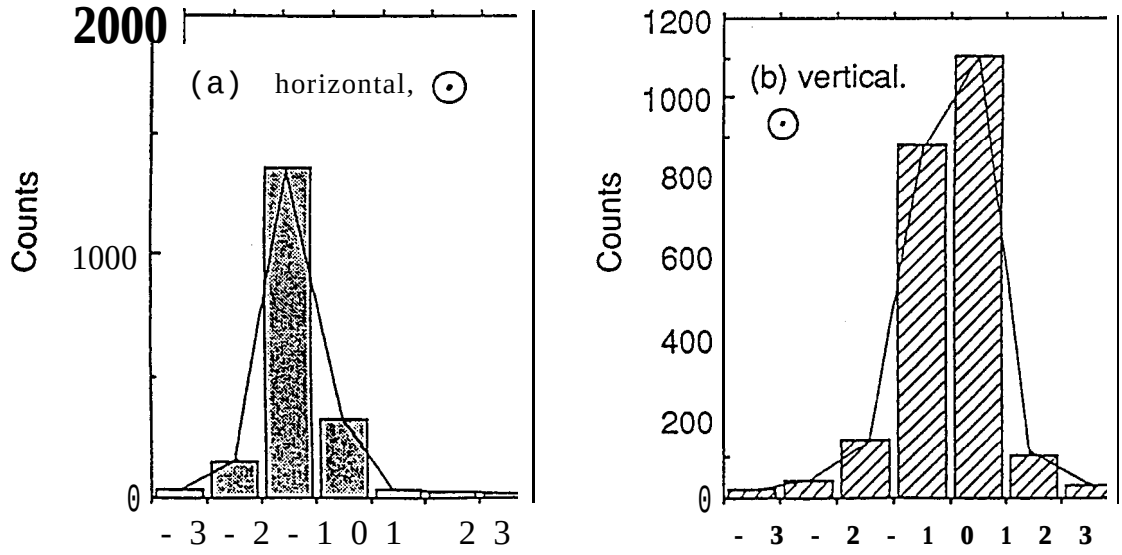

Figure 2. Horizontal and vertical distribution of ^{24}Na yield in the Al foil at the beam entrance hole. The width of the histogram corresponds for 1 cm. The circles indicates that the protons were injected from the bottom of the paper.

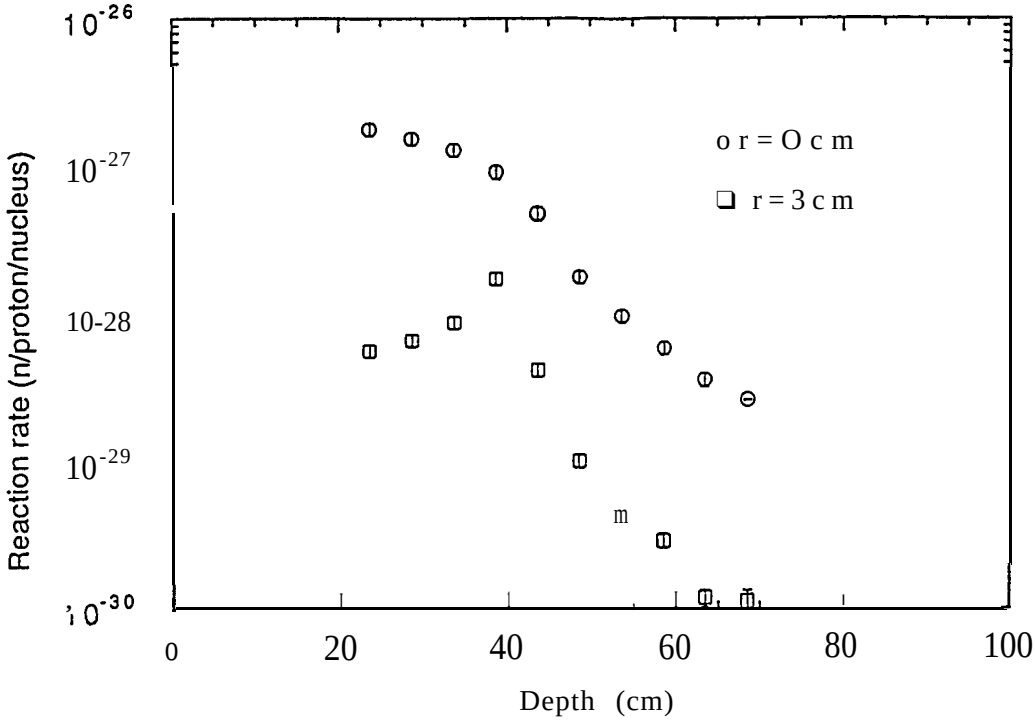

Figure 3. Spatial distribution of the reaction rate for ^{206}Bi produced in the lead samples for 500 MeV protons injected in the lead assembly.

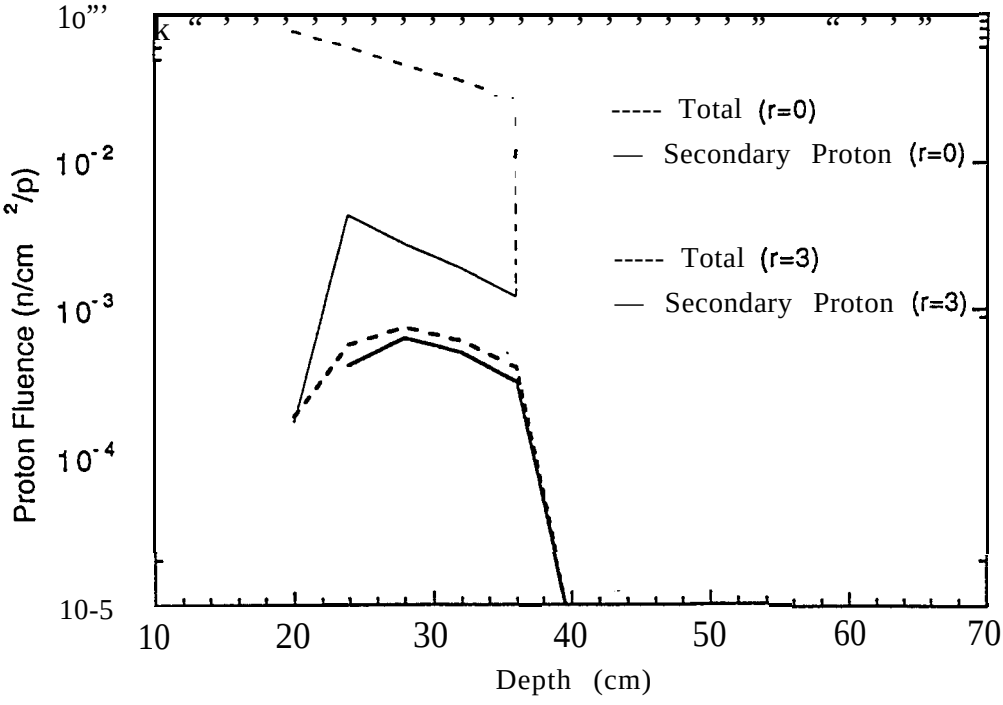

Figure 4. Proton fluence in the lead assembly calculated by the surface cross estimation method using NMTC/JAERI for 500 MeV proton incidence. The dashed lines stand for the number of the total protons. The solid ones represent the one of the secondary protons.

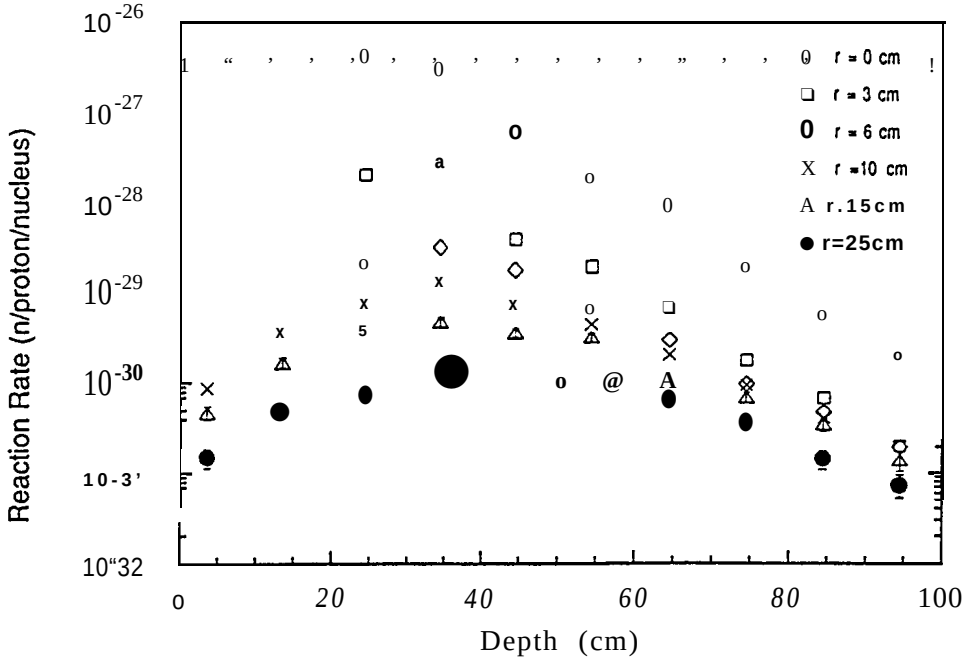

Figure 5. Spatial distribution of the reaction rate for 57Ni produced in the nickel samples for 500 MeV proton incidence on the lead assembly.

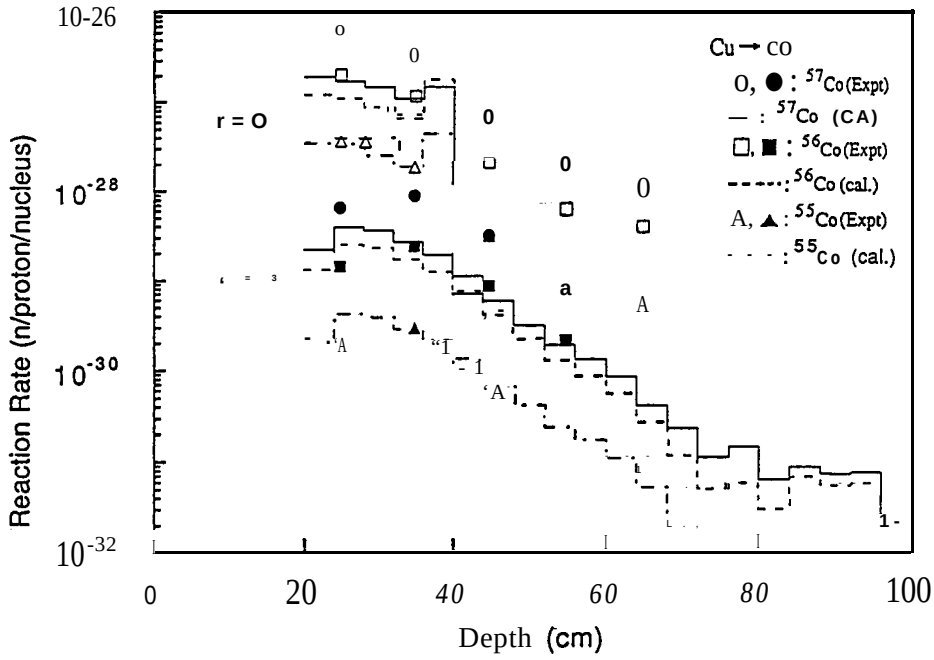

Figure 6. Spatial distribution of the reaction rate for ^{57}Co, ^{56}Co and 55C0 produced in the copper samples for 500 MeV proton incidence on the lead assembly. The open and the solid marks stand for the measured data at r=O and 3 cm, respectively. The solid, the dotted and the dot-dashed lines represent the calculated results for ^{57}Co, ^{56}Co and 55C0 by NMTC/JAERI, respectively.

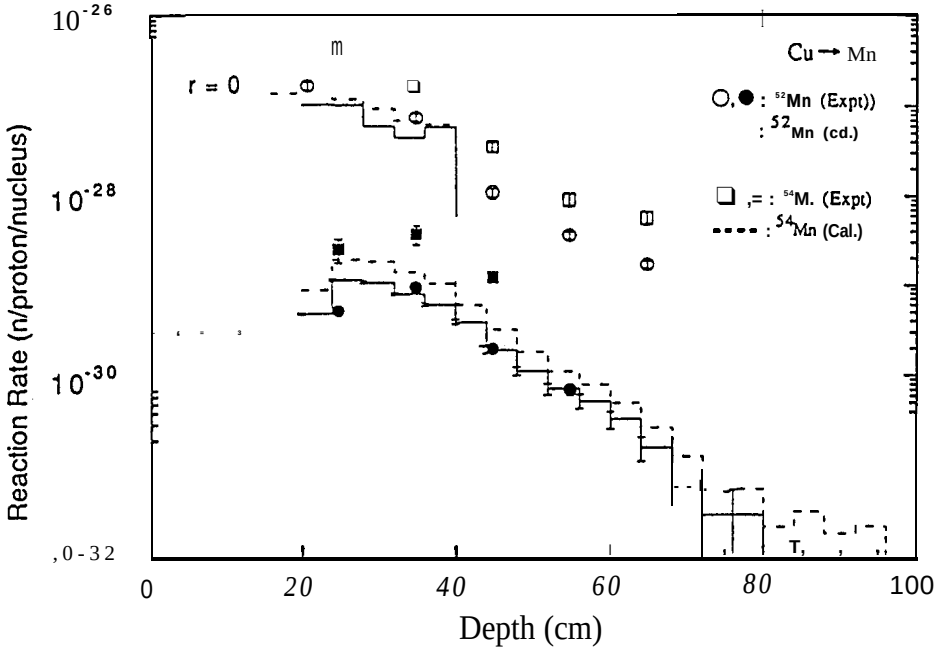

Figure 7. Spatial distribution of the reaction rate for ^{54}Mn and ^{52}Mn produced in the copper samples for 500 MeV proton incidence on the lead assembly. The open and the solid marks stand for the measured data for ^{54}Mn and ^{52}Mn, respectively. The solid and the dotted lines represent the calculated results for ^{54}Mn and ^{52}Mn by NMTC/JAERI, respectively.

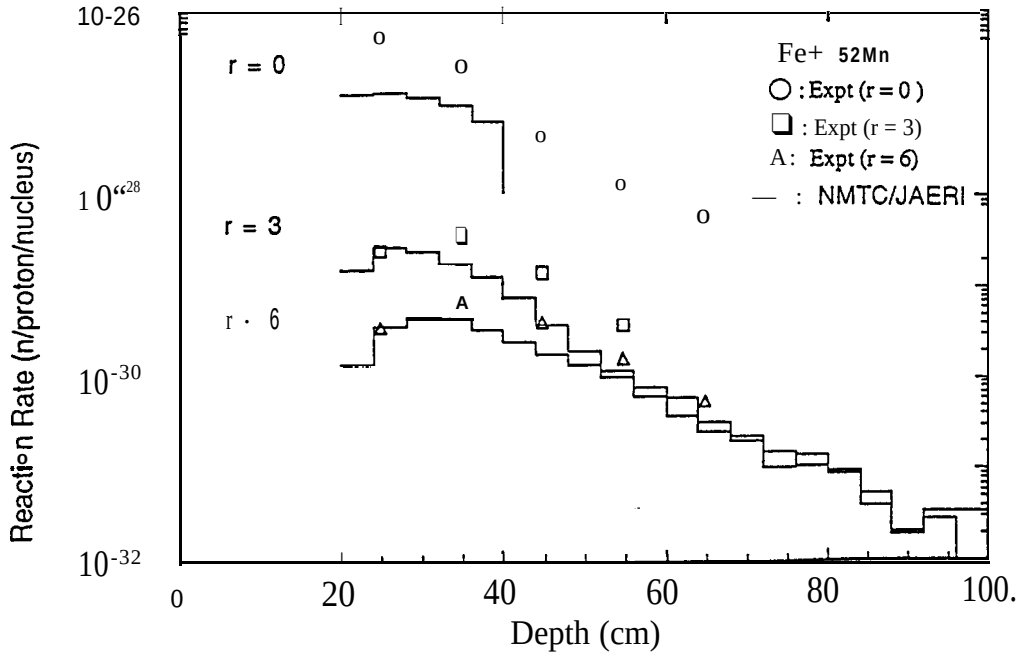

Figure 8. Spatial distribution of the reaction rate for ^{52}Mn produced in the iron samples for 500 MeV proton incidence on the lead assembly. The open marks stand for the measured data. The solid lines indicate the calculated results by NMTC/JAERI.

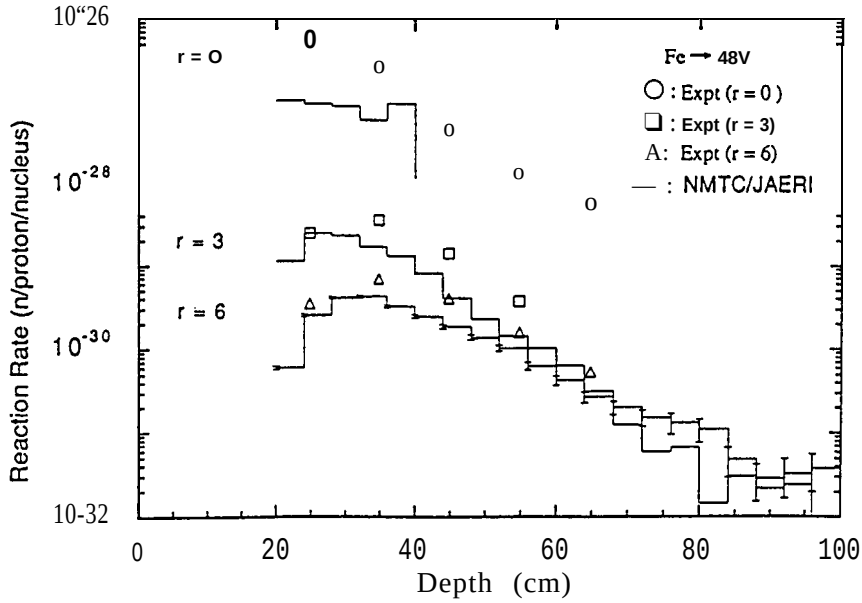

Figure 9. Spatial distribution of the reaction rate for ^{48}V produced in the iron samples for 500 MeV proton incidence on the lead assembly. The open marks stand for the measured data. The solid lines indicate the calculated results by NMTC/JAERI.

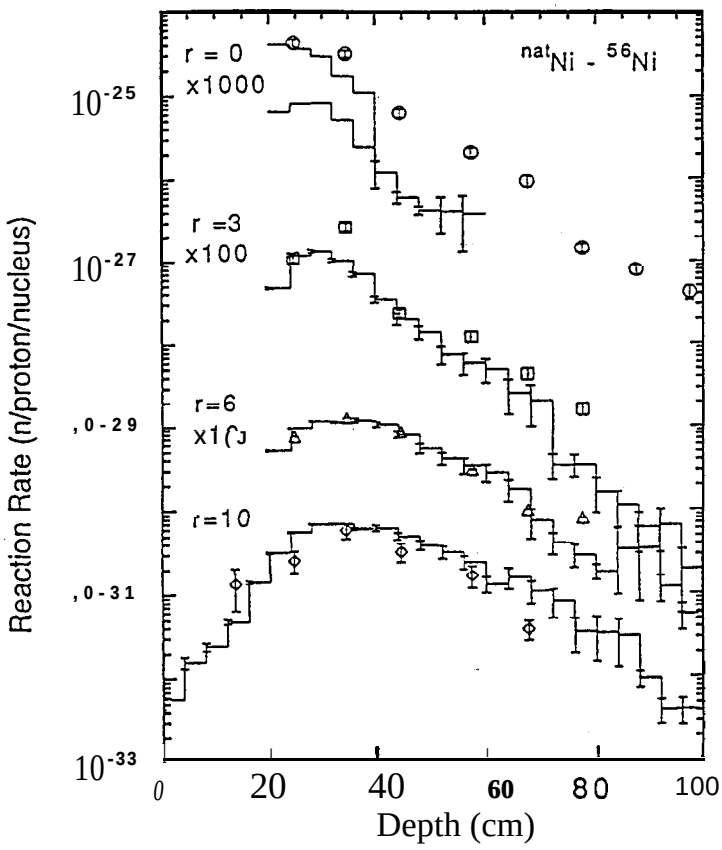

Figure 10. Spatial distribution of the reaction rate for ^{56}Ni produced in the nickel samples for 500 MeV proton incidence on the lead assembly. The open marks stand for the measured data. The solid lines indicate the calculated results by NMTC/JAERI.

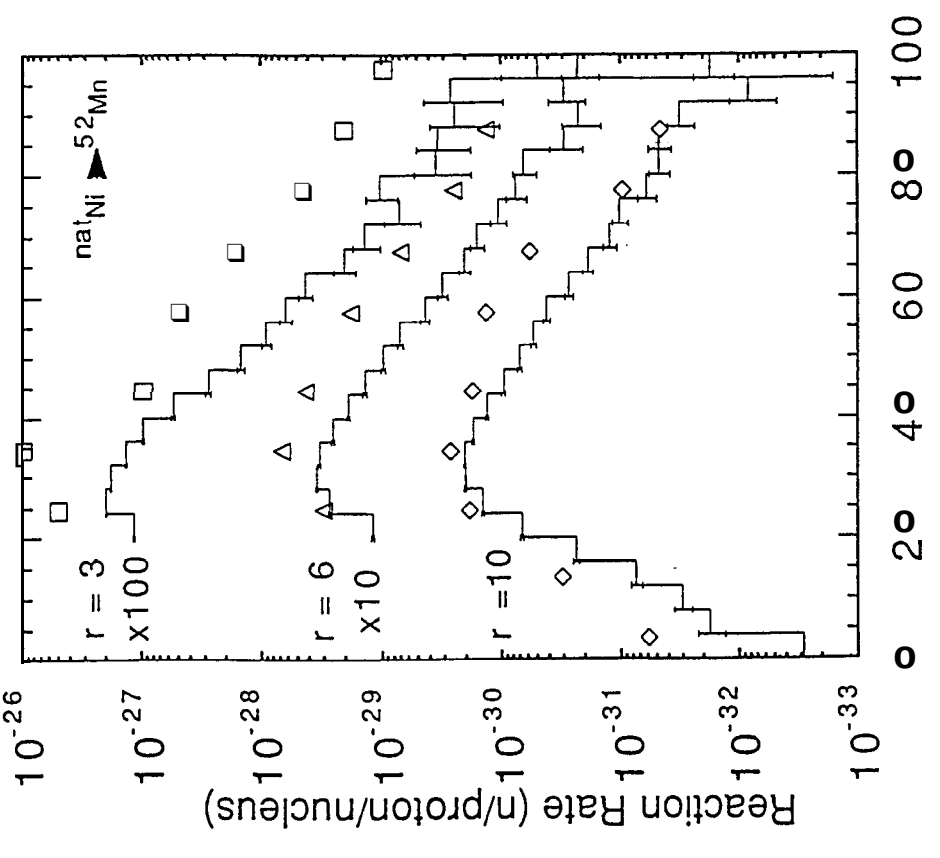

Figure 11. Spatial distribution of the reaction rate for ^{52}Mn produced in the nickel samples for 500 MeV proton incidence on the lead assembly. The open marks stand for the measured data. The solid lines indicate the calculated results by NMTC/JAERI.

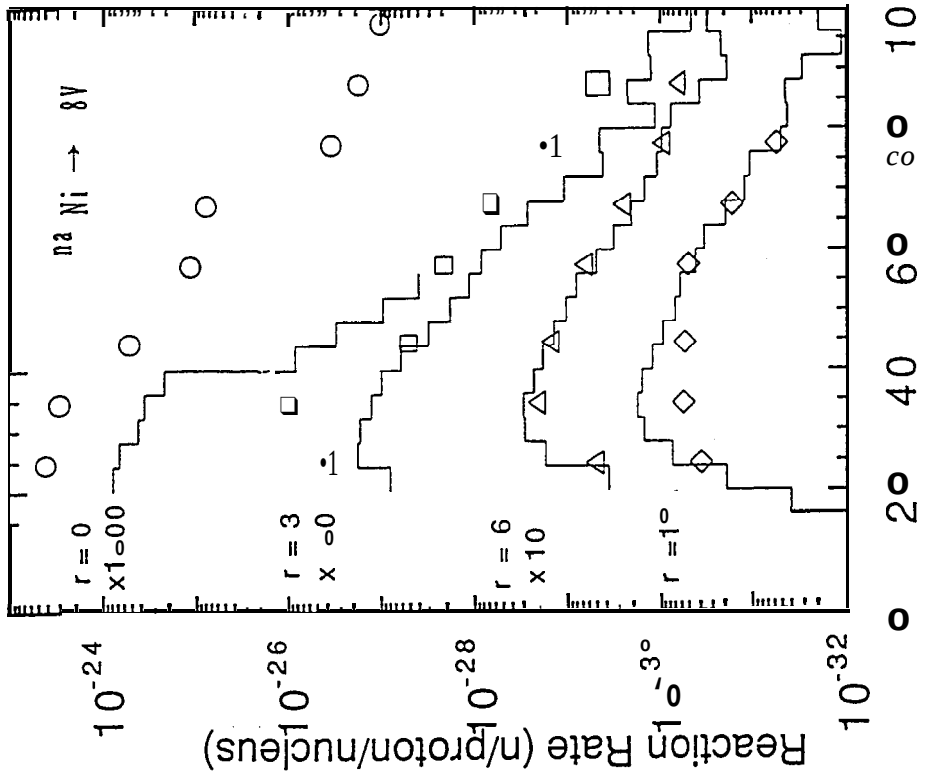

Figure 12. Spatial distribution of the reaction rate for ^{48}V produced in the nickel samples for 500 MeV proton incidence on the lead assembly. The open marks stand for the measured data. The solid lines indicate calculated the results by NMTC/JAERI.

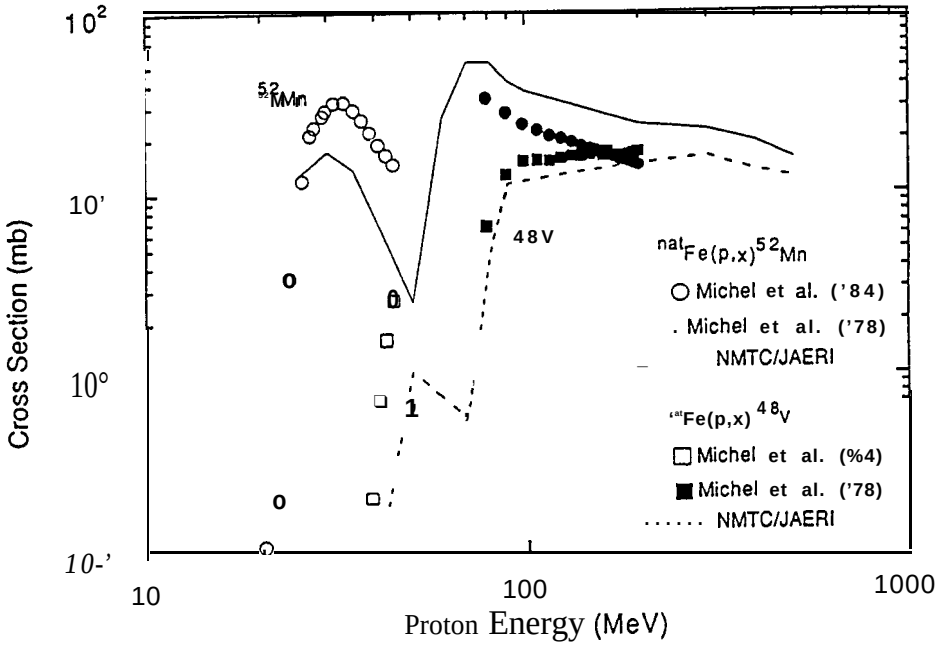

Figure 13. Excitation function of ^{52}Mn and ^{48}V for the proton incidence on iron. The circles and the squares stand for the experimental data by Michel et al.(16,17) for ^{52}Mn and ^{48}V, respectively. The solid and the dotted lines represent the calculated results by NMTC/JAERI for ^{52}Mn and ^{48}V, respectively.

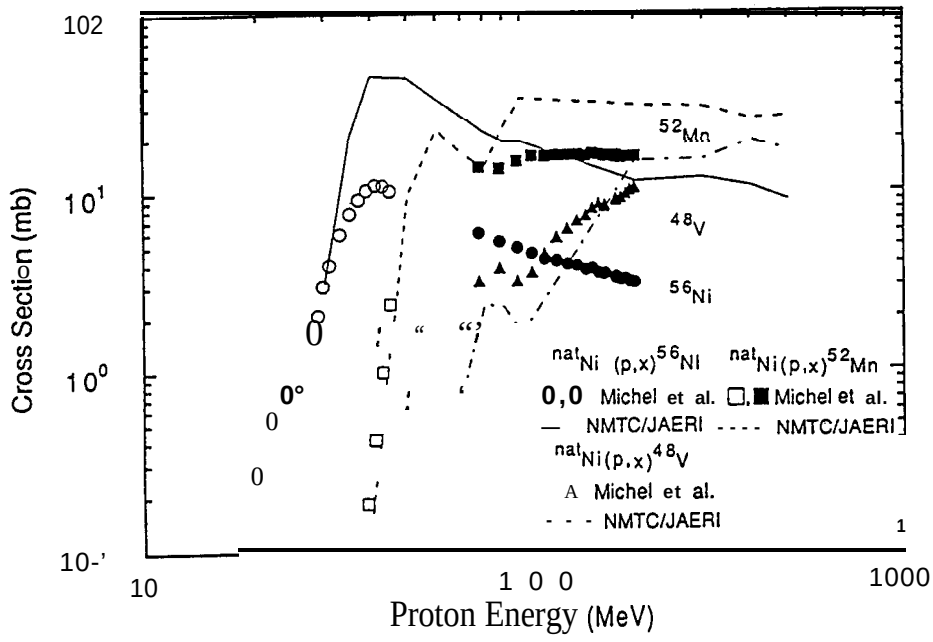

Figure 14. Excitation function of ^{56}Ni, ^{52}Mn and ^{48}V for the proton incidence on nickel. The circles, the squares and the triangles stand for the experimental data by Michel et al.(15,17) for ^{56}Ni, ^{52}Mn and ^{48}V, respectively. The solid, the dotted and the dot-dashed lines represent the calculated results by NMTC/JAERI for ^{56}Ni, ^{52}Mn and ^{48}V, respectively.